Acta Crystallographica Section F
Structural Biology and Crystallization Communications
ISSN 1744-3091

ATP-dependent DNA ligase from *Thermococcus* sp. 1519 displays a new arrangement of the OB-fold domain

T. Petrova,[a,b]* E. Y. Bezsudnova,[a] K. M. Boyko,[a,c] A. V. Mardanov,[d] K. M. Polyakov,[b,e] V. V. Volkov,[f] M. Kozin,[f] N. V. Ravin,[d] I. G. Shabalin,[a] K. G. Skryabin,[c,d] T. N. Stekhanova,[a] M. V. Kovalchuk[c,f] and V. O. Popov[a,c]

[a]Bach Institute of Biochemistry, RAS, Leninsky pr. 33, Moscow 119071, Russian Federation, [b]Institute of Mathematical Problems of Biology, RAS, Institutskaja str. 4, Pushchino 142290, Russian Federation, [c]RSC 'Kurchatov Institute', Acad. Kurchatov sq. 1, Moscow 123182, Russian Federation, [d]Centre 'Bioengineering', RAS, Prosp. 60-let Oktyabrya, bld. 7-1, Moscow 117312, Russian Federation, [e]Engelhardt Institute of Molecular Biology, RAS, Vavilov str. 32, Moscow 119991, Russian Federation, and [f]Shubnikov Institute of Crystallography, RAS, Leninsky pr. 59, Moscow 119333, Russian Federation

Correspondence e-mail: petrova@impb.psn.ru

Received 7 September 2012
Accepted 18 October 2012

PDB Reference: LigTh1519, 3rr5

DNA ligases join single-strand breaks in double-stranded DNA by catalyzing the formation of a phosphodiester bond between adjacent 5′-phosphate and 3′-hydroxyl termini. Their function is essential for maintaining genome integrity in the replication, recombination and repair of DNA. High flexibility is important for the function of DNA ligase molecules. Two types of overall conformations of archaeal DNA ligase that depend on the relative position of the OB-fold domain have previously been revealed: closed and open extended conformations. The structure of ATP-dependent DNA ligase from *Thermococcus* sp. 1519 (LigTh1519) in the crystalline state determined at a resolution of 3.02 Å shows a new relative arrangement of the OB-fold domain which is intermediate between the positions of this domain in the closed and the open extended conformations of previously determined archaeal DNA ligases. However, small-angle X-ray scattering (SAXS) measurements indicate that in solution the LigTh1519 molecule adopts either an open extended conformation or both an intermediate and an open extended conformation with the open extended conformation being dominant.

1. Introduction

DNA ligases catalyze the sealing of adjacent 5′-phosphate and 3′-hydroxyl termini at single-stranded breaks in double-stranded DNA. Their function is crucial in DNA replication, recombination and repair (Lehman, 1974). The reaction catalyzed by DNA ligases proceeds by three sequential nucleotidyl-transfer steps. In the first step, the active-site lysine is activated by the covalent attachment of AMP, which is accompanied by the release of pyrophosphate or nicotinamide mononucleotide from the cofactor (ATP or NAD^+). AMP is then transferred to the 5′-end of the 5′-phosphate-terminated DNA strand to form DNA adenylate. In the final step, the phosphodiester bond is formed with concomitant release of AMP from the DNA-adenylate intermediate. DNA ligases are present in all living organisms and are conventionally divided into two families according to their cofactor specificity (Sriskanda *et al.*, 2000). The first group contains ATP-dependent ligases (EC 6.5.1.1), which are found in eukaryotes, archaea, viruses and some bacteria. The second group comprises NAD^+-dependent DNA ligases (EC 6.5.1.2); these are present in bacteria and some eukaryotic viruses.

DNA ligases from thermophilic and hyperthermophilic archaea have been used as model systems in structural and mechanistic studies of DNA ligation. A number of thermostable DNA ligases from archaea have been isolated and functionally characterized (Sriskanda *et al.*, 2000; Lai *et al.*, 2002; Keppetipola & Shuman, 2005). All of them utilized ATP as a cofactor and it was generally accepted that archaeal DNA ligases belong to the family of ATP-dependent ligases. However, it was subsequently found that some DNA ligases from hyperthermophilic euryarchaea of the order Thermococcales (*Thermococcus kodakarensis*, *T. fumicolans*, *T. onnurineus* and *Pyrococcus abyssi*) are also able to use NAD^+ as a cofactor (Nakatani *et al.*, 2000; Rolland *et al.*, 2004; Kim *et al.*, 2006). Therefore, it was suggested that the dual specificity of Thermococcales DNA ligases reflects an intermediate phase in the evolution of an ancestral enzyme into the cofactor-specific specialized present-day enzymes (Sun *et al.*, 2008).

Table 1
Experimental setup and statistics of data collection and processing.

Values in parentheses are for the highest resolution shell.

Space group	$P2_12_12_1$
Radiation source	National Research Center 'Kurchatov Institute'
Unit-cell parameters (Å)	a = 76.950, b = 85.600, c = 105.960
Temperature (K)	100
Wavelength (Å)	0.800
Crystal-to-detector distance (mm)	410
Oscillation range (°)	0.5
Mosaicity (°)	0.20
No. of frames	720
Resolution limit (Å)	29.26–3.02 (3.20–3.02)
Total reflections	68411 (10505)
Molecules per asymmetric unit	1
Solvent content (%)	55
Independent reflections	13339 (2121)
Average $I/\sigma(I)$	14.19 (1.75)
Completeness (%)	93.3 (94.0)
R_{merge}	0.10 (0.66)

Only a few crystal structures of archaeal DNA ligases have been reported: those from the Euryarchaeota *P. furiosus* (PfuLig; Nishida *et al.*, 2006), *Archaeoglobus fulgidus* (AfuLig; Kim *et al.*, 2009) and *T. sibiricus* (TsibLig; Petrova *et al.*, 2012) and the Crenarchaeota *Sulfolobus solfataricus* (SsoLig; Pascal *et al.*, 2006) and *Sulfophobococcus zilligii* (Supangat *et al.*, 2010). Previously, we identified and functionally characterized the ATP-dependent DNA ligase from the hyperthermophilic archaeon *Thermococcus* sp. 1519 from the order Thermococcales (LigTh1519; Smagin *et al.*, 2008). We succeeded in the crystallization and structure determination of this enzyme at 2.9 Å resolution (Bezsudnova *et al.*, 2009) and found a molecular-replacement solution for two domains only. We suggested that the third domain, the OB-fold domain, either adopted different positions in different cells of the crystal or was hydrolyzed during crystallization. Subsequently, we collected X-ray data from a crystal of LigTh1519 grown under different conditions. Here, we report the results of a crystallographic study of the ATP-dependent DNA ligase from *Thermococcus* sp. 1519 with all three domains. A comparative analysis of the structures of ATP-dependent DNA ligases may help in the identification of sites for directed mutagenesis aimed at changing the cofactor specificity of the enzyme from ATP to NAD.

2. Materials and methods

Expression and purification have previously been described by Bezsudnova *et al.* (2009).

2.1. Crystallization

Freshly prepared recombinant LigTh1519 (22.1 mg ml^{-1}) in 50 m*M* Tris–HCl pH 7.5 containing 100 m*M* NaCl and 0.5 m*M* DTT was used. Initial crystallization screening of LigTh1519 was performed at 291 K by the hanging-drop vapour-diffusion method using Crystal Screen, Index and Crystal Screen Cryo kits (Hampton Research). A single crystal was obtained after six months using the gel-tube counter-diffusion method at 291 K. The truncated square bipyramidal crystal had dimensions of about 200–300 µm. The reservoir solution consisted of 0.1 *M* sodium cacodylate pH 6.5, 0.2 *M* $MgCl_2$, 20% glycerol, 16% PEG 8000, 100 m*M* NaCl, 50 m*M* Tris–HCl pH 7.5.

2.2. X-ray data collection and treatment

X-ray diffraction data were collected on beamline BL41XU at the Spring-8 synchrotron using a MAR Mosaic 225 mm CCD detector. A crystal was flash-cooled in a stream of cold nitrogen gas at 100 K. Data collection was performed using the *HKL*-2000 software package (Otwinowski & Minor, 1997). Experimental details are summarized in Table 1. X-ray diffraction images were indexed, integrated and subsequently scaled using *HKL*-2000. Data reduction was performed using the *CCP*4 package (Winn *et al.*, 2011). Data-collection statistics are given in Table 1.

SAXS measurements were performed at a wavelength of 0.1542 nm using an AMUR-K diffractometer with an OD3M linear position-sensitive detector and a graphite monochromator. The Kratky-type geometry was used with a sample-to-detector distance of 700 mm and a sample slit width of 0.2 mm to cover the range of momentum transfer $0.12 < s < 12.0$ nm^{-1} ($s = 4\pi\sin\theta/\lambda$, where 2θ is the scattering angle). Measurements were carried out at room temperature for 2 h using sample solutions placed in 1 mm quartz capillaries. The data were normalized to the intensity of the incident beam and corrected for X-ray absoption and collimation distortions using standard procedures (Feigin & Svergun, 1987).

Table 2
Refinement statistics.

R_{work}/R_{free}	0.233/0.310
R.m.s. deviations from ideal geometry	
Bond lengths (Å)	0.009
Bond angles (°)	1.319
Average B factor (Å^2)	
Main-chain atoms	84.3
Side-chain atoms	84.2
Ramachandran plot (%)	
Most favourable	95.8
Allowed	3.8
Outliers	0.4

2.3. Structure determination and refinement

The structure of LigTh1519 was solved using *BALBES* (Long *et al.*, 2008). The best solution found by *BALBES* was obtained using the PfuLig model (PDB entry 2cfm; Nishida *et al.*, 2006) as a starting model for molecular replacement and refinement. The model was further refined using *phenix.refine* (Afonine *et al.*, 2005). The refined parameters were the coordinates for each atom and the *B* factors for groups of atoms. The relatively small number of observations did not allow us to refine *B* factors for each atom. Two *B* factors were refined for each residue: one for the atoms of the main chain and the other for the side-chain atoms. Along with a set of standard stereochemical restraints, secondary-structure restraints and Ramachandran restraints were applied during refinement. Examination of density maps and the manual rebuilding of the model were performed using the program *Coot* (Emsley & Cowtan, 2004).

In addition to a LigTh1519 molecule, the final model contained four water molecules and one Mg^{2+} ion. There was no interpretable electron density for 11 N-terminal residues, including six purification-tag residues, and six C-terminal residues. The geometry of the final model was inspected by *PROCHEC*K (Laskowski *et al.*, 1993). A summary of the refinement statistics and model quality is given in Table 2. Atomic coordinates and experimental structure factors were deposited in the Protein Data Bank and are accessible as entry 3rr5.

3. Results and discussion

3.1. Overall conformation of the LigTh1519 molecule

Like previously determined molecules of ATP-dependent DNA ligases, the LigTh1519 molecule comprises three domains: an N-terminal DNA-binding domain (DBD), an adenylation domain

(AdD) and a C-terminal OB-fold domain (OBD) (Fig. 1*a*). Previously, the following conformations of ATP-dependent DNA ligases have been determined depending on the relative position of the OBD.

(i) Closed conformation. This conformation was revealed for PfuLig (Nishida *et al.*, 2006; PDB entry 2cfm; Fig. 1*b*), AfuLig (Kim *et al.*, 2009; PDB entry 3gde) and TsibLig (Petrova *et al.*, 2012; PDB entry 4eq5).

(ii) Open extended conformation. This conformation was displayed by SsoLig (Pascal *et al.*, 2006; PDB entries 2hiv and 2hix; Fig. 1*c*).

(iii) Open conformation. This conformation was displayed by human DNA ligase I bound to DNA (Pascal *et al.*, 2004; PDB entry 1x9n) and human DNA ligase III bound to DNA (Cotner-Gohara *et al.*, 2010; PDB entry 3l2p).

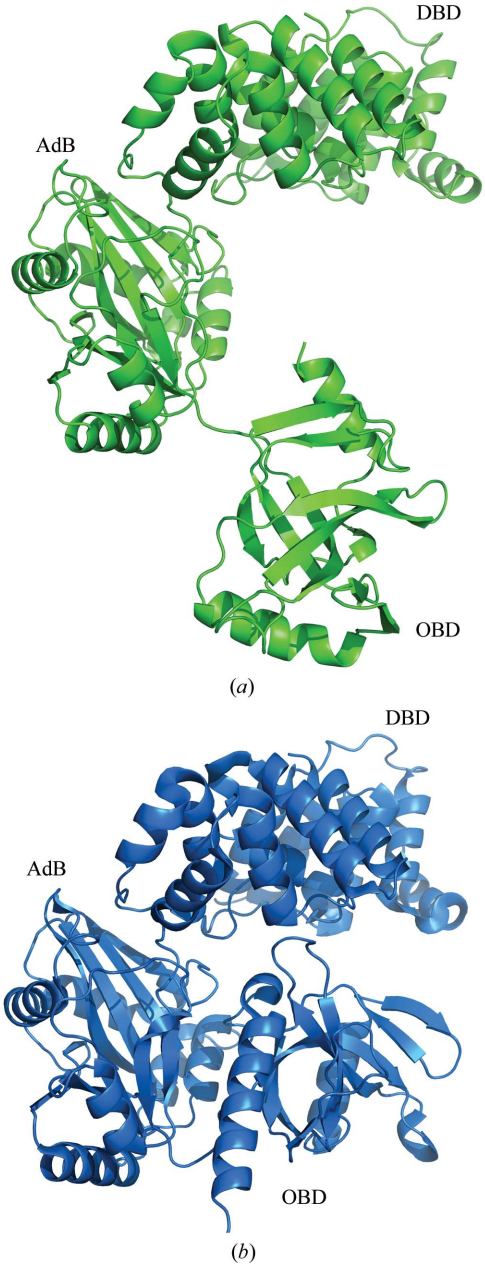

Thus, only two conformations have previously been revealed for archaeal DNA ligases: the closed and open extended conformations.

The LigTh1519 molecule in the crystalline state shows a new relative arrangement of the OBD which is intermediate between the positions of this domain in the open extended and closed conformations of DNA ligases (Fig. 2). To derive this new intermediate position from that corresponding to the open extended conformation, the OBD should be rotated in the anticlockwise direction by approximately 90° around the AdD (Fig. 2*a*). Further rotation of the OBD around a slightly different axis by about 120° in the anticlockwise direction leads to the position that corresponds to the closed conformation (Fig. 2*b*). The position of the OBD in LigTh1519 rather resembles the position of the OBD in the two-domain DNA ligases from Chlorella virus (PDB entry 1p8l; Odell *et al.*, 2003) and from bacteriophage T7 (PDB entry 1a0i; Subramanya *et al.*, 1996) (Figs. 2*c* and 2*d*). Note that while the relative position of the OBD differs significantly in the open extended, closed and intermediate conformations, the relative positions of the DBD and AdD are very similar. The r.m.s.d.s calculated over C^{α} atoms of the first two domains, DBD and AdD, for superimposed molecules of LigTh1519 and PfuLig and of LigTh1519 and SsoLig are 1.3 and 2.2 Å, respectively.

Interestingly, unlike other DNA ligases from archaea, the OBD in LigTh1519 is not connected to the other two domains through hydrogen bonds and salt bridges; the only link between the OBD and the rest of the molecule is a covalent bond. It appears as if the OBD is floating around the AdD. In the crystal, this position of the OBD is fixed by eight hydrogen bonds and three salt bridges to the AdD of a symmetry-related molecule (Figs. 3*a* and 3*b*). Note that the residues involved in these interactions form the only contact region between the OBD and the other domains and fix the position of the OBD in the crystal structure. The side chains of these residues are easily

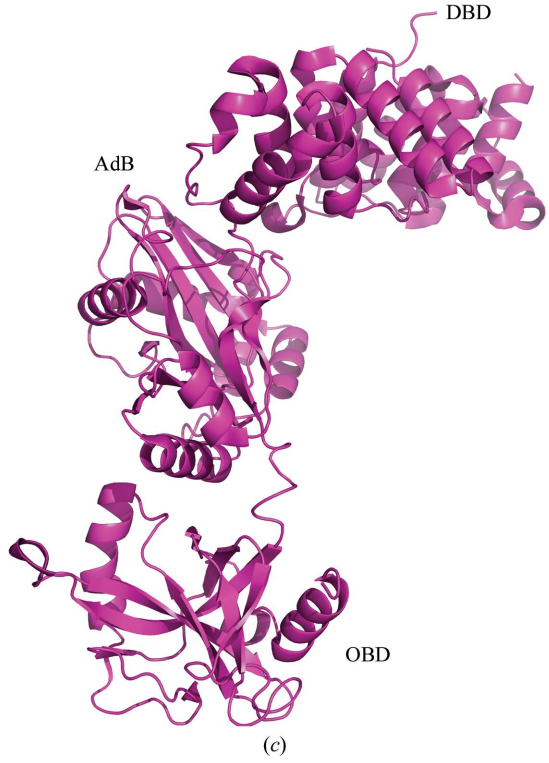

Figure 1
Different conformations of archaeal DNA ligases. (*a*) A ribbon diagram of LigTh1519, which shows a new position of the OBD; (*b*) a ribbon diagram of PfuLig, which shows a closed conformation; (*c*) a ribbon diagram of SsoLig, which shows an open extended conformation.

visible in the electron-density map. It seems that the position of the OBD is stabilized by these interactions.

The final model of LigTh1519 did not contain an ATP molecule. Although ATP was not externally added to the crystallization solution, it might have copurified with the ligase (as in PfuLig and TsibLig). Therefore, the final structure may be a complex of the enzyme with endogenous ATP. The relatively poor electron density did not allow unambiguous determination of whether or not an ATP molecule was present in the active site. In addition, Arg280, the conformation of which was determined unambiguously, would be too close to the possible position of the cofactor (Fig. 4)

In all three DNA ligases that adopt the closed conformation, PfuLig, TsibLig and AfuLig, the conformation of the corresponding Arg residue differs from that observed in the LigTh1519 structure. Note that PfuLig and TsibLig contain an ATP molecule and AfuLig contains phosphate ions in the active site. The position of the corresponding Arg residue in SsoLig, which adopts the open extended conformation and contains no cofactor in the active site, is

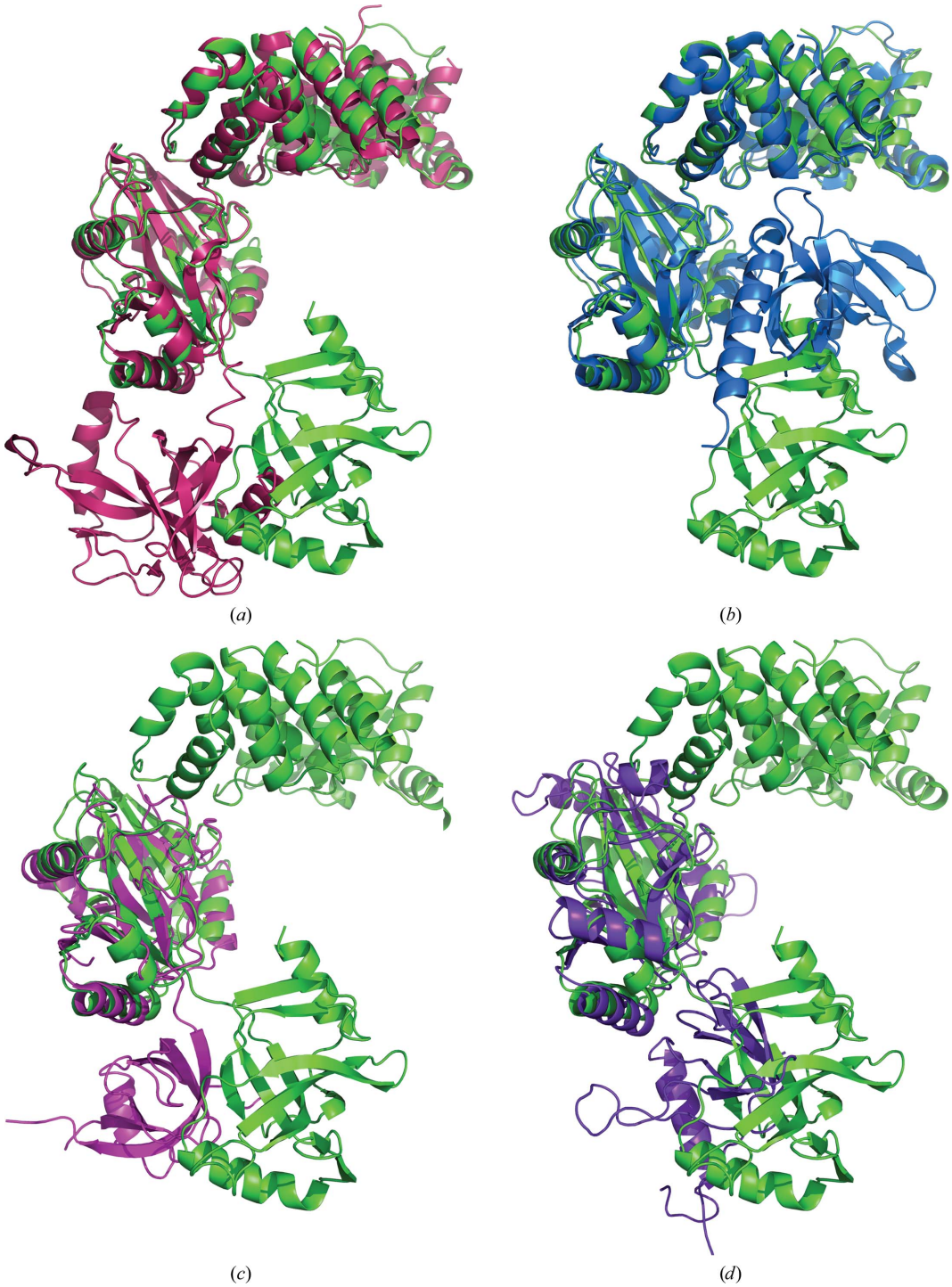

Figure 2
Superposition of LigTh1519 (green) with (*a*) SsoLig (pink), (*b*) PfuLig (blue), (*c*) Clorella virus DNA ligase (magenta) and (*d*) DNA ligase from bacteriophage T7 (violet).

different and is much closer to the conformation of Arg280 in LigTh1519 (Fig. 4).

3.2. Comparison of the OBD arrangement in PfuLig and LigTh1519

PfuLig has very high sequence similarity (79%) to LigTh1519; the similarity between their OBDs is 85%. However, the relative positions of the OBDs in the crystal structures differ significantly. Using the *PISA* server at the European Bioinformatics Institute (http://www.ebi.ac.uk/pdbe/prot_int/pistart.html; Krissinel & Henrick, 2007), we revealed those amino-acid residues in the structure of PfuLig that

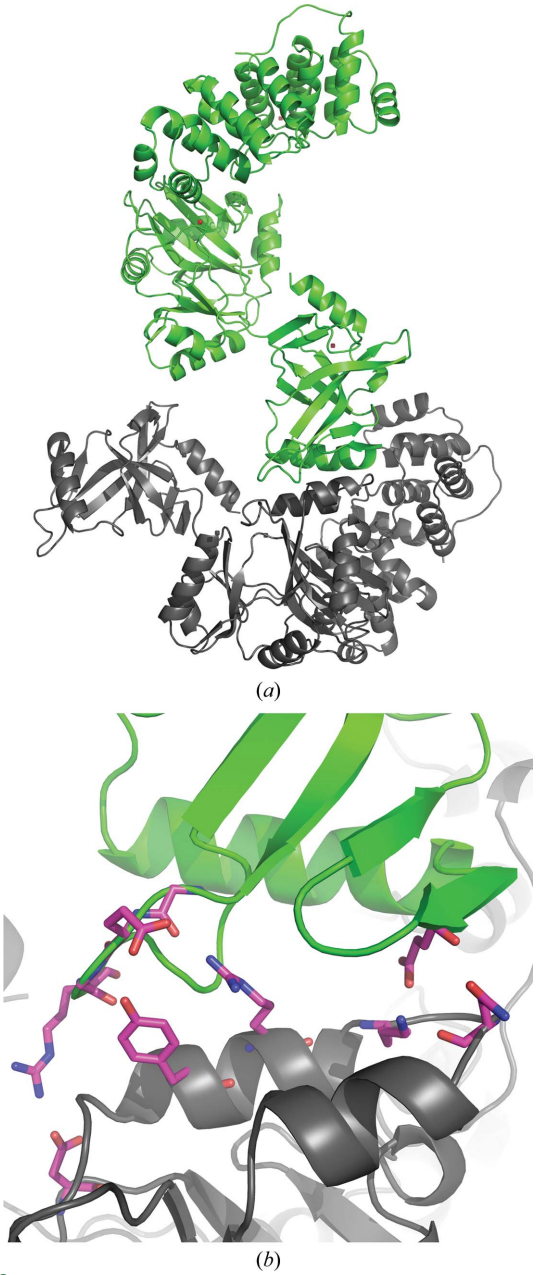

Figure 3
The OBD of LigTh1519 (green) and a symmetry-related molecule (grey) in the crystal. (*a*) The OBD of LigTh1519 is only covalently bound to the rest of the molecule. In the crystal, the position of the OBD is fixed by a symmetry-related molecule. (*b*) An enlarged view of the region between the OBD and the AdD of a symmetry-related molecule. Residues participating in hydrogen bonds between the OBD and the AdD of a symmetry-related molecule are shown in stick representation.

Table 3
Hydrogen bonds and salt bridges in PfuLig.

Residues that are also present in LigTh1519 are shown in plain text. A few residues that are not present in LigTh1519 but for which there are residues with similar properties in the equivalent positions are shown in italics. Note that residues in equivalent positions in the models of PfuLig and LigTh1519 have different numbers.

(*a*) Hydrogen bonds and salt bridges between the AdD and the OBD.

No.	OBD residue atom	Distance (Å)	AdB residue atom
1	Glu426 N	3.08	*Gln229* OE1
2	Lys554 NZ	3.89	*Asp235* OD2
3	Thr424 O	2.93	*Gln229* NE2
4	Glu426 OE1	2.56	Lys420 NZ
5	Glu426 OE2	3.88	Lys249 NZ
6	Val528 O	3.78	Gln313 NE2
7	Asp532 O	3.02	Arg270 NH1
8	*Asp532* OD1	2.84	Arg320 NH1
9	Asp533 O	2.84	Arg270 N
10	Lys534 O	3.55	Arg270 NH1
11	Asp540 OD1	3.53	Arg414 NH2
12	Asp532 OD2	3.81	Arg320 NE
13	Asp532 OD2	3.21	Arg320 NH1

(*b*) Hydrogen bonds and salt bridges between the DBD and the OBD.

No.	OBD residue atom	Distance (Å)	DdB residue atom
1	Tyr454 OH	2.55	Glu168 OE2
2	*Glu457* OE1	2.53	Arg172 NH2
3	*Glu457* OE2	3.26	Arg172 NH1
4	*Glu457* OE1	3.03	Arg172 NH1

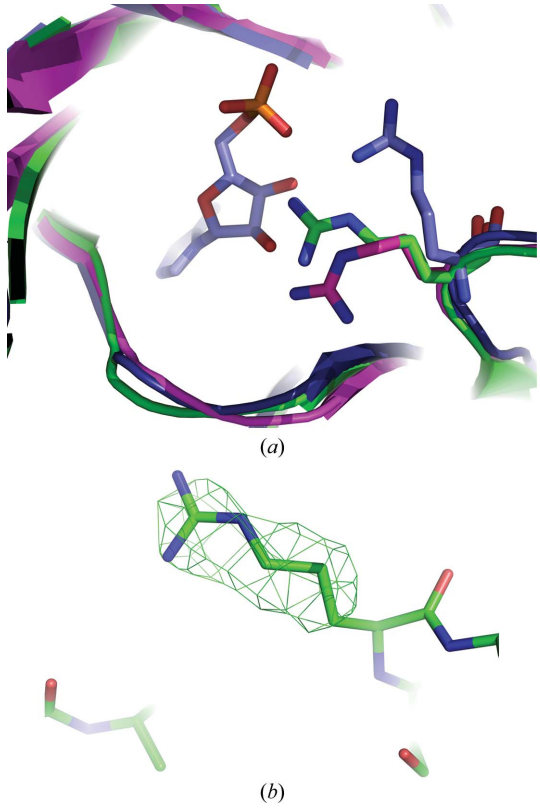

Figure 4
Superposition of the active sites of LigTh1519 (green), PfuLig (blue) and SsoLig (magenta). (*a*) The conformation of Arg280 in LigTh1519 is significantly different from the conformation of Arg269 in PfuLig, which is in the closed conformation and contains an AMP molecule in the active site. The conformations of Arg280 in LigTh1519 and in SsoLig, which is in the open extended conformation, are different, although not significantly. (*b*) An $F_{obs} - F_{calc}$ OMIT map of the side chain of Arg280 confirms the position of the side chain of Arg280. The map is shown in green and contoured at the 2.5σ level.

participate in hydrogen-bond contacts and salt bridges between the OBD and the other two domains. Alignment of the PfuLig and the LigTh1519 sequences shows that most of the residues are present in the same positions in the structure of LigTh1519 (Table 3). A few residues (shown in italics in Table 3) at equivalent positions in LigTh1519 and PfuLig are homologues with similar properties (Glu457→Asp468, Gln229→Asn240, Asp235→Glu246 and Asp532→Glu543).

The PfuLig molecule contains a C-terminal extension helix (residues 541–561) which passes through the cleft between the AdD and the OBD and contributes, mainly through ionic interactions, to the link between these two domains. Nishida *et al.* (2006) proposed that the C-terminal extension helix in the PfuLig structure plays a crucial role in stabilizing the closed conformation. In the C-terminal parts of PfuLig and LigTh1519 only two residues differ. In the structure of LigTh1519 seven terminal residues are disordered and, as a result, the terminal helix is shorter than that in the PfuLig structure. In fact, the superposition of the OBDs of PfuLig and LigTh1519 shows that the terminal part of the C-terminal extension helix would overlap with residues of the AdD of LigTh1519 in the vicinity of the active site.

Thus, the difference between the sequences of PfuLig and LigTh1519 cannot explain the difference in the arrangement of the OBD. In other words, it seems that there is nothing that prevents the LigTh1519 molecule from adopting the closed conformation.

3.3. Comparison of the OBD arrangement in SsoLig and LigTh1519

The sequence similarity between SsoLig and LigTh1519 is considerably lower (40%) than that between PfuLig and LigTh1519. Alignment of the SsoLig and the LigTh1519 sequences reveals that the hinge between the AdD and the OBD in the SsoLig structure comprises eight amino acids, while in the LigTh1519, PfuLig and AfuLig structures the hinge involves only six amino acids. The larger hinge might favour the open extended conformation in the crystal structure of SsoLig and may explain why this conformation is not observed in the crystal structures of PfuLig and LigTh1519. In addition, the arrangement of the OBD in the structure of SsoLig is fixed by numerous hydrogen bonds and salt bridges between the OBD and the AdD (Table 4). With the exception of Arg564 (shown in bold in Table 4), the enumerated residues or their homologues are present at the same positions in LigTh1519.

3.4. SAXS experiment

An SAXS experiment was performed in order to reveal the conformation of LigTh1519 in solution.

The scattering intensity from known PDB structures was calculated using *CRYSOL* (Svergun *et al.*, 1995), which takes the scattering from the excluded volume and hydration shell into account. The scattering curve calculated from the SsoLig structure is in better agreement with the experimental intensities than the scattering curve calculated from LigTh1519 (Fig. 5*a*, Table 5).

The pair-distance distribution functions $p(r)$ were calculated from experimental intensities using *GNOM* (Svergun *et al.*, 1988). The radius of gyration R_g was calculated using the Guinier approximation (Guinier, 1939) at $sR_g < 1.5$,

$$I_{exp}(s) \simeq I(0)\left[1 - \frac{s^2}{3} \cdot R_g^2\right], \quad (1)$$

and the relation (*International Tables for Crystallography*, 1992)

Table 4
Hydrogen bonds and salt bridges between the AdD and the OBD in SsoLig.

Residues that are present in LigTh1519 are shown in plain text. Ser398, Ile404 and Ser405 (shown in italics) are not present in LigTh1519; residues with similar properties are present at the equivalent positions. Arg564 (shown in bold) is not present in LigTh1519; Ala540 is at the equivalent position. Note that residues in equivalent positions in the models of SsoLig and LigTh1519 have different numbers.

No.	OBD residue atom	Distance (Å)	AdB residue atom
1	Arg561 NH1	3.24	Glu394 OE1
2	Arg561 NH2	2.71	Glu394 OE2
3	Arg561 NH1	3.65	*Ser398* OG
4	Arg561 NH2	3.18	Glu394 OE1
5	**Arg564** NH2	3.84	*Ile404* O
6	**Arg564** NH2	2.66	*Ser405* O
7	Gly488 O	2.86	Arg402 NH1
8	Gln493 OE1	2.72	Arg402 NH1

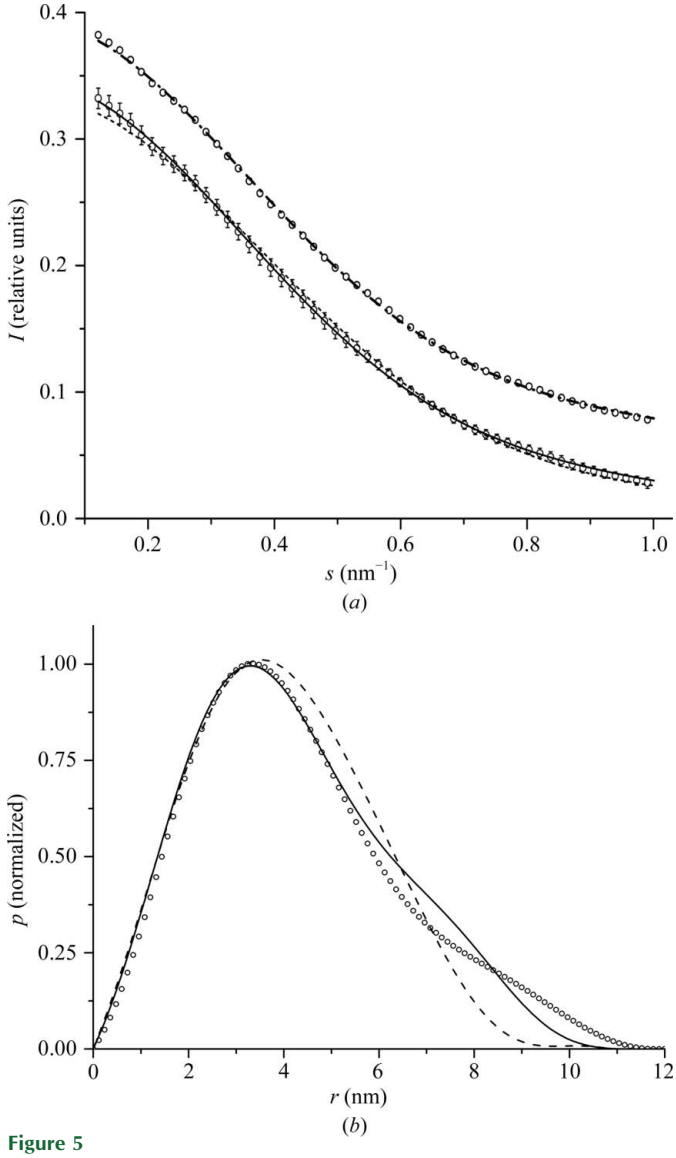

Figure 5
Results of the SAXS experiment. (*a*) SAXS intensity profiles for the experimental data (circles) and calculated from models of SsoLig (continuous line) and LigTh1519 (dashed line) and a mixture of the SsoLig (81%) and LigTh1519 (19%) models (dashed/dotted line). The scattering profile for the mixture is shifted vertically by 0.05. The experimental profile is shown twice; one of the copies is also shifted vertically by 0.05 for comparison with the profile for the mixture. (*b*) Normalized pair-distance distribution functions calculated from experimental SAXS data (circles) and from models of SsoLig (continuous line) and LigTh1519 (dashed line) in the crystalline state.

Table 5
Structural parameters derived from SAXS experimental data and calculated from the models of SsoLig and of LigTh1519 in the crystalline state and a mixture of the SsoLig and LigTh1519 models.

R_g is the radius of gyration and D_{max} is the maximum interatomic distance.

	R_g (nm)	D_{max} (nm)	χ^2 experiment–model
SAXS experimental data	3.4 ± 0.05	11.5 ± 0.5	—
SsoLig	3.3 ± 0.01	10.8 ± 0.2	0.84
LigTh1519	3.1 ± 0.01	9.2 ± 0.2	1.1
Mixture of the SsoLig (81 ± 3%) and LigTh1519 (19 ± 3%) models	3.28 ± 0.01 (averaged value)	—	0.78

$$R_g^2 \simeq \frac{\int_0^D r^2 p(r)\,dr}{2\int_0^D p(r)\,dr}. \quad (2)$$

Estimate (2) is much less influenced by aggregation effects, because relatively large aggregates significantly increase the scattering intensity only at small angles, thus increasing estimate (1). The approximately equal values, 3.40 ± 0.05 and 3.41 ± 0.05 nm, obtained from (1) and (2), respectively, indicate that aggregation was negligibly small. The maximal size D_{max} of dissolved molecules (or the maximal interatomic distance) was estimated from the profile of the $p(r)$ function.

The graph for the normalized distance-distribution function and structural parameters calculated from SAXS experimental data are much closer to those calculated for the SsoLig model than to those of LigTh1519 (Fig. 5*b* and Table 5). The right shoulder on the experimental distribution curve indicates the presence of relatively large distances intrinsic to the open extended conformation of the protein. Thus, we concluded that the LigTh1519 molecule adopts an open extended conformation in solution, but not the conformation that it shows in the crystalline state. We also checked whether the experimental data can be fitted to the data calculated for a mixture of SsoLig and LigTh1519 form factors using the program *OLIGOMER* (Konarev *et al.*, 2003). The results showed (see Table 5 and Fig. 5*a*) that a somewhat better fit to the experimental data was attained for the mixture of SsoLig (81%) and LigTh1519 (19%). Thus, LigTh1519 molecules might exist in both conformations in solution, with scattering from the molecule in the open extended conformation being dominant.

3.5. A new intermediate conformation of ATP-dependent DNA ligase

The structure of LigTh1519 was studied using X-ray crystallography in combination with SAXS and comparative structure analysis with known archaeal ATP-dependent DNA ligases. A new conformation of LigTh1519 was revealed which is intermediate between the open extended and closed conformations. Taking the absence of bound or trapped ATP or phosphate ions in the LigTh1519 structure into account, in contrast to PfuLig, TsibLig or AfuLig, we might consider this intermediate conformation of LigTh1519 as a structural variation of the open extended conformation. In the LigTh1519 crystal the absence of stabilizing hydrogen bonds between the OBD and the AdD is partially compensated for by hydrogen bonds and salt bridges between the OBD and the neighbouring symmetry-related molecules; the OBD is additionally fixed by eight intermolecular hydrogen bonds and three intermolecular salt bridges.

Previously, based on the strikingly different positions of the OBD in different DNA ligases, a conclusion was made about high OBD flexibility, which is essential for the function of DNA ligases. Moreover, if the respective movement of the AdD and the OBD is restricted, the efficiency of adenylation will be reduced (Ochi *et al.*, 2012). Here, we report further experimental evidence for this high flexibility. The amino-acid composition, the structural arrangement of the catalytic domains (AdD and OBD) and the presence of ligands do not explain the advantage of the open, closed or intermediate conformations for DNA-free enzymes in crystals. However, the SAXS experiment showed that the LigTh1519 molecule in solution predominantly adopts the open extended conformation, thereby fixing the OBD and providing additional stabilization of the whole structure in an aqueous environment.

This work was supported by the Ministry of Education and Sciences of Russia (contract 02.740.11.0765 and grant NS 7200.2012.4).

References

Afonine, P. V., Grosse-Kunstleve, R. W. & Adams, P. D. (2005). *CCP4 Newsl.* **42**, contribution 8.

Bezsudnova, E. Y., Kovalchuk, M. V., Mardanov, A. V., Poliakov, K. M., Popov, V. O., Ravin, N. V., Skryabin, K. G., Smagin, V. A., Stekhanova, T. N. & Tikhonova, T. V. (2009). *Acta Cryst.* F**65**, 368–371.

Cotner-Gohara, E., Kim, I.-K., Hammel, M., Tainer, J. A., Tomkinson, A. E. & Ellenberger, T. (2010). *Biochemistry*, **49**, 6165–6176.

Emsley, P. & Cowtan, K. (2004). *Acta Cryst.* D**60**, 2126–2132.

Feigin, L. A. & Svergun, D. I. (1987). *Structure Analysis by Small-Angle X-ray and Neutron Scattering*, p. 363. New York: Plenum Press.

Guinier, A. (1939). *Ann. Phys. (Paris)*, **12**, 161–236.

International Tables for Crystallography (1992). Vol. *C*, *Mathematical, Physical and Chemical Tables*, 1st ed., edited by A. J. C. Wilson, p. 91. Dordrecht/Boston/London: Kluwer Academic Publishers.

Keppetipola, N. & Shuman, S. (2005). *J. Bacteriol.* **187**, 6902–6908.

Kim, D. J., Kim, O., Kim, H.-W., Kim, H. S., Lee, S. J. & Suh, S. W. (2009). *Acta Cryst.* F**65**, 544–550.

Kim, Y. J., Lee, H. S., Bae, S. S., Jeon, J. H., Yang, S. H., Lim, J. K., Kang, S. G., Kwon, S.-T. & Lee, J.-H. (2006). *Biotechnol. Lett.* **28**, 401–407.

Konarev, P. V., Volkov, V. V., Sokolova, A. V., Koch, M. H. J. & Svergun, D. I. (2003). *J. Appl. Cryst.* **36**, 1277–1282.

Krissinel, E. & Henrick, K. (2007). *J. Mol. Biol.* **372**, 774–797.

Lai, X., Shao, H., Hao, F. & Huang, L. (2002). *Extremophiles*, **6**, 469–477.

Laskowski, R. A., MacArthur, M. W., Moss, D. S. & Thornton, J. M. (1993). *J. Appl. Cryst.* **26**, 283–291.

Lehman, I. R. (1974). *Science*, **186**, 790–797.

Long, F., Vagin, A. A., Young, P. & Murshudov, G. N. (2008). *Acta Cryst.* D**64**, 125–132.

Nakatani, M., Ezaki, S., Atomi, H. & Imanaka, T. (2000). *J. Bacteriol.* **182**, 6424–6433.

Nishida, H., Kiyonari, S., Ishino, Y. & Morikawa, K. (2006). *J. Mol. Biol.* **360**, 956–967.

Ochi, T., Wu, Q., Chirgadze, D. Y., Grossmann, J. G., Bolanos-Garcia, V. M. & Blundell, T. L. (2012). *Structure*, **20**, 1212–1222.

Odell, M., Malinina, L., Sriskanda, V., Teplova, M. & Shuman, S. (2003). *Nucleic Acids Res.* **31**, 5090–5100.

Otwinowski, Z. & Minor, W. (1997). *Methods Enzymol.* **276**, 307–326.

Pascal, J. M., O'Brien, P. J., Tomkinson, A. E. & Ellenberger, T. (2004). *Nature (London)*, **432**, 473–478.

Pascal, J. M., Tsodikov, O. V., Hura, G. L., Song, W., Cotner, E. A., Classen, S., Tomkinson, A. E., Tainer, J. A. & Ellenberger, T. (2006). *Mol. Cell*, **24**, 279–291.

Petrova, T. E., Bezsudnova, E. Y., Dorokhov, B. D., Slutskaya, E. S., Polyakov, K. M., Dorovatovskiy, P. V., Ravin, N. V., Skryabin, K. G., Kovalchuk, M. V. & Popov, V. O. (2012). *Acta Cryst.* F**68**, 163–165.

Rolland, J.-L., Gueguen, Y., Persillon, C., Masson, J.-M. & Dietrich, J. (2004). *FEMS Microbiol. Lett.* **236**, 267–273.

Smagin, V. A., Mardanov, A. V., Bonch-Osmolovskaia, E. A. & Ravin, N. V. (2008). *Prikl. Biokhim. Mikrobiol.* **44**, 523–528.

Sriskanda, V., Kelman, Z., Hurwitz, J. & Shuman, S. (2000). *Nucleic Acids Res.* **28**, 2221–2228.

Subramanya, H. S., Doherty, A. J., Ashford, S. R. & Wigley, D. B. (1996). *Cell*, **85**, 607–615.

Sun, Y., Seo, M. S., Kim, J. H., Kim, Y. J., Kim, G. A., Lee, J. I., Lee, J.-H. & Kwon, S.-T. (2008). *Environ. Microbiol.* **10**, 3212–3224.
Supangat, S., An, Y. J., Sun, Y., Kwon, S.-T. & Cha, S.-S. (2010). *Acta Cryst.* F**66**, 1583–1585.
Svergun, D., Barberato, C. & Koch, M. H. J. (1995). *J. Appl. Cryst.* **28**, 768–773.
Svergun, D. I., Semenyuk, A. V. & Feigin, L. A. (1988). *Acta Cryst.* A**44**, 244–250.
Winn, M. D. *et al.* (2011). *Acta Cryst.* D**67**, 235–242.